



Research Article

Effects of electric field, MHD micropolar hybrid nanofluid flow with mixed convection and thermal radiation across a flat surface

Aruna J.¹, H. NIRANJAN^{1,*}

¹Department of Mathematics, School of Advanced Sciences, Vellore Institute of Technology, Vellore, Tamilnadu, 632014, India

ARTICLE INFO

Article history

Received: 09 January 2024

Revised: 08 April 2024

Accepted: 09 April 2024

Keywords:

Electric Field; Hybrid Nanofluid; Micropolar Fluid; Mixed Convection; MHD; Thermal Radiation

ABSTRACT

Hybrid nanofluids significantly impact the thermal properties of pure fluids. This study examines the flow of a micropolar electrically conducting hybrid nanofluid in a mixed convective MHD environment over a flat surface. The enclosed fluid is a specialized water-based mixture of hybrid nanoparticles containing silver and alumina, uniformly dispersed to fill the enclosure. Suction and injection effects are applied to the vertically positioned plate within a permeable material. Further considerations include Joule heating, electrical effects, thermal radiation, and viscous dissipation. The nonlinear PDEs are converted into a dimensionless form and subsequently solved numerically using the `bvp4c` function in MATLAB. Results show increased fluid mobility with magnetic and mixed convection factors, declining under micropolar component presence. Micropolar parameters enhance fluid micro rotational velocity. Thermal behavior diminishes with the higher electric field and rises with increased magnetic effects, heat source, radiation, Eckert number, and micropolar parameter. The velocity curve elevates with a higher electric field factor. The Nusselt number and dimensionless skin friction coefficient values are computed and graphically represented. The research finds applications in engineering and medicine, including Heat Exchangers, Microfluidics, Medical Imaging, Electroplating, and Electrokinetic Pumps. Electric field effects are pivotal in electrothermal thrusters for spacecraft propulsion, leveraging principles of magnetohydrodynamics (MHD) and hybrid nanofluid flow to enhance performance in the vacuum space.

Cite this article as: J. A, Niranjana H. Effects of electric field, MHD micropolar hybrid nanofluid flow with mixed convection and thermal radiation across a flat surface. J Ther Eng 2024;10(6):1607–1620.

INTRODUCTION

Hybrid nanofluid refers to a fluid where various types of nanoparticles are dissolved in a base fluid. The basic fluid's thermal conductivity, heat transfer coefficient, and viscosity can be improved by adding nanoparticles of variable shapes

and materials. It can improve the efficiency of electrical devices, lubricate mechanical systems, aid in drug delivery in biomedical engineering, and increase heat transfer in thermal systems, among other uses. Jamil and Ali [1] found that hybrid nanofluids are better than standard thermal transfer fluid-like such as water, ethylene glycol, oil, and

*Corresponding author.

*E-mail address: niranjana.hari@vit.ac.in

This paper was recommended for publication in revised form by Editor-in-Chief Ahmet Selim Dalkılıç



nanofluids having one nanoparticle. Suneetha et al. [2] discussed how Hybrid nanofluids are employed in solar power, nuclear cooling, and healthcare. Chu et al. [3] examined the thermal conduction analysis involving a hybrid nanofluid including four nanoparticle kinds. They found how the electromagnetic field angle of inclination lowers the mobility profile. Khan et al. [4] investigated the steady convection motion of $SiO_2-Al_2O_3/H_2O$ nanofluid hybridization around a stationary point with a curving edge. Kayalvizhi and Vijaya Kumar [5] examined entropy generation in a hybrid nanofluid flowing towards a stretched surface, finding that magnetic field and porous media parameters decrease the velocity boundary layer, while electric field E behaves differently. In a separate study, Mandal [6] investigated water/Ag-MgO nanofluid stability and entropy over a permeable Riga surface, considering slip and convective boundary circumstances. Roy et al., Paul et al. and Singh et al. [7–9] primarily investigated heat transfer in hybrid fluids, likely exploring factors like fluid composition and flow conditions on heat transfer properties.

The microstructural effects of a micropolar fluid are caused by the rotation of its constituent particles. Micropolar fluids exhibit distinct flow behaviours and extra transport phenomena due to their consideration of the internal structure and rotation of tiny particles. Rheology, the study of matter flow and deformation, biomedicine, the research of complicated fluid behaviour in microcirculation, and materials science all make use of micropolar fluids. Eringen [10] Explains the micropolar fluid concept first. Several academics described micropolar fluids' uses in practice. Lone et al. [11] studied flat-surface mixed convection MHD micropolar hybrid nanofluid flow. Investigators found that bigger micropolar variables boost fluid micro-rotational velocity. Zaib et al. [12] investigate micropolar magnetite Fe_3O_4 Ferro-liquid off an inclined surface utilizing mixed convection flow. Tripathi et al. [13] studied blood flow microrotation results. Bansal et al. [14] found micropolar liquids effective as lubricants due to lower friction coefficients compared to Newtonian fluids. Tanuja et al. [15] explored heat transport mechanisms in porous channels with micropolar liquids, noting higher temperatures in hybrid nanofluids than clear or binary hybrids. Shah et al. [16] studied magnetic and electric field effects on micropolar nanofluids among rotating plates, observing increased velocity distribution with greater Reynolds numbers. Khan et al. [17] looked into micro-rotation and heat transfer characteristics near stagnation points, noting initial friction factor increase followed by a decline with suction, with the steady improvement of heat transfer and micro-rotation gradient. Previous studies Ram et al., Roja et al., Alqahtani et al., Mollamahdi et al. and Jawad et al. [18–22] extensively examined mass and heat transmission in micropolar hybrid nanofluids, covering various parameters and geometrical configurations, providing a comprehensive understanding.

Joule heating happens when electrical currents flow through a material, causing the substance's resistance to

transform the energy from the current into heat. Heat transmission properties and temperature distribution in the hybrid nanofluid might be affected by Joule heating. Electric heating elements in appliances, resistance heating in industrial operations like welding, and component bonding and soldering in electronics are just a few of the many uses for this versatile compound. This concept was first found by Joule [23]. Khan et al. [24] Examined Lorentz's force-driven chemically reactive flow of Darcy-Forchheimer viscous fluid using a stretching curved sheets entropy optimizing. Saeed et al. [25] reviewed the transportation heat-related stress couple models using EMHD, heat absorbing, Joule warming, and viscous dispersal. Shamshuddin et al. [26] developed a model for processing magnetic polymers based on their research into the unstable reacting magnet radiant micropolar flow, heat, with mass transfer through an inclined plate using Joule heating.

The term "Thermal radiation" describes the electromagnetic waves emitted by a hot surface. Where there are temperature gradients across a flat surface, thermal radiation becomes much more important in heat transfer processes. It has several applications, including infrared heating in home appliances, passive solar heating in structures, and thermal imaging in fields as diverse as medicine and industry. Pramanik [27] Thermal radiation raises effective thermal diffusivity with the border layer's temperature gradients towards a not-Newtonian liquid under heat exchange onto an exponentially increasing area under sucking. Hassan and Fenuga [28] studied thermal radiation's impact on reacting hydromagnetic couple pressure fluid via a passable channel driven by a heat source. He found that thermal radiation significantly affects motion, with magnetic strength slowing it down and fluid temperature decreasing due to thickness. Reddy et al. [29] investigated the effect of a magnetic field on the motion of a non-uniform magnetic hydrodynamic nanofluid in a porous medium across an infinite flat plate subjected to a ramping temperature gradient. Srilatha et al. [30] examined the impact of slip boundary conditions on the rates of mass and heat exchange through the analysis of micropolar MHD flow across a porous stretched surface.

The process of viscous dissipation happens when the viscosity or internal friction of a flowing fluid causes mechanical energy to be transformed into heat. When this happens, the fluid undergoes a transformation that changes its flow behaviour and how its temperature is distributed. Important areas of application include fluid dynamics (for studying pipeline energy losses), lubrication engineering (for figuring out bearing and gear losses), and materials processing (for managing temperature gradients in liquid metals). Jakeer et al. [31] determined the entropy process of EMHD hybrid nanofluid on the point of stagnation with slip, production of heat, and fluid dissipation. They found that greater magnetized parameters as well as Ec numbers increase entropy generation. Abbas et al. [32] compared hybrid nanofluid with traditional nanofluid in a micropolar fluid environment under MHD conditions, analyzing

rotating porous channels on an exponentially stretched surface. The researchers observed that a hybrid nanofluid demonstrates higher rates of heat transmission in comparison to the conventional nanofluid.

The novelty of our research lies in its pioneering exploration of the intricate interactions between electric fields and MHD micropolar hybrid nanofluid flow dynamics, complemented by the incorporation of mixed convection and thermal radiation phenomena across a flat surface. By delving into these complex interactions, our study aims to provide a deeper understanding of how electric field influences the behavior of MHD micropolar hybrid nanofluids, offering valuable insights into the combined effects of electric fields, mixed convection, and thermal radiation on fluid flow and thermal conduction processes. This holistic approach to investigating fluid dynamics and heat transmission across a flat surface sets our research apart, paving the way for novel advancements in the field. Graphically, portray temperature, velocity, and micro rotation profiles for varied parameters. The following research gaps will be filled in by the end of the project:

- How do electric field and thermal radiation change the profile of temperature and velocity of a micropolar hybrid nanofluid ($Ag-Al_2O_3 / H_2O$) across a flat surface?
- How does the electric field influence the micro rotational velocity within the micropolar hybrid nanofluid ($Ag-Al_2O_3 / H_2O$) system?
- How do the various fixed values influence the rates of skin friction and heat transfer?

This research offers a variety of important real-time applications across engineering and medical domains such as heat exchangers, electrohydrodynamics (EHD) pumps and cooling systems, thermal management in electronics, intracellular manipulation and targeted therapies and electroplating and Surface Coating. To tackle these research inquiries with a focus on practical applications, our study focused on an electromagnetic field coupled with micropolar hybrid nanofluid flow close to a stagnation point that contains nanoparticles of alumina and silver.

PHYSICAL AND MATHEMATICAL FORMULATION

Consider the stagnation point of a mixed convection MHD stream in a micropolar electrically conducting hybrid nanofluid. Keep the surface vertical and normal to the y -axis. Gravitational acceleration (g) and velocity components in the region, denoted by $u(x,y)$ and $v(x,y)$, are considered. We mix silver (Ag) and Alumina (Al_2O_3) in water. B_0 and E_0 represents the magnetic and electric fields' normal flow direction as depicted in Figure 1.

To solve this, the following assumptions are made:

- At the stagnation point, micropolar fluid is considered. Mixed convection and heat source effects are used in the flow system.
- Considered effects include joule heating, thermal radiation, viscosity dissipation, and suction/injection.

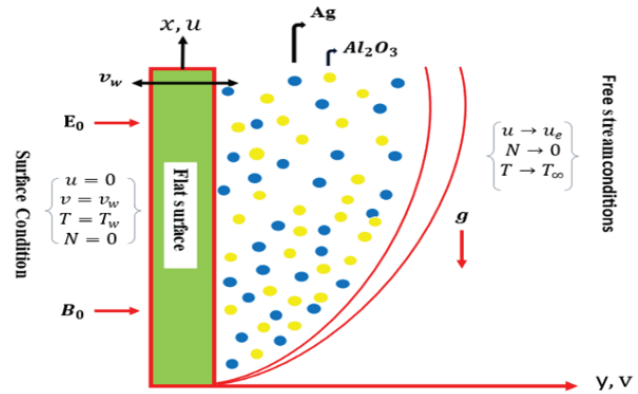


Figure 1. Structure of the problem.

- $u_e(x) = cx$ is for the ambient motion, where the constant c is a positive number.
- The surface temperature of the sheet is denoted by $T_w(x) = T_\infty + bx$, where T_∞ and b stands for the surrounding temperature and constant, respectively.

The modelled problem assumes the following form under the assumptions above [11, 33, 34]:

$$u_x + v_y = 0 \tag{1}$$

$$uu_x + vv_y = u_e u_{e_x} + \frac{1}{\rho_{hnf}} (\mu_{hnf} + K_1) u_{yy} + \frac{K_1}{\rho_{hnf}} N_y + \frac{\sigma_{hnf}}{\rho_{hnf}} (E_0 B_0 - B_0^2 (u - u_e)) + g \frac{(\rho\beta)_{hnf}}{\rho_{hnf}} (T - T_\infty) \tag{2}$$

$$uN_x + vN_y = \frac{\gamma_{hnf}}{\rho_{hnf}} N_{yy} - \frac{K_1}{\rho_{hnf} j} (2N + u_y) \tag{3}$$

$$uT_x + vT_y = \frac{k_{hnf}}{(\rho C_p)_{hnf}} T_{yy} - \frac{1}{(\rho C_p)_{hnf}} q_r + \frac{Q_0}{(\rho C_p)_{hnf}} (T - T_\infty) + \frac{\mu_{hnf}}{(\rho C_p)_{hnf}} (u_y)^2 + \frac{\sigma_{hnf}}{(\rho C_p)_{hnf}} (B_0 u - E_0)^2 \tag{4}$$

In the Equation above 4, q_r (Radiant heat flux) can be written in mathematical notation as [35, 36]:

$$q_r = - \left(\frac{4\sigma^*}{3k^*} T_y^4 \right) \tag{5}$$

T^4 is simplified using the Taylor expansion to be:

$$T^4 \cong 4TT_\infty^3 - 3T_\infty^4 \tag{6}$$

The Energy Equation (4) is rewritten as follows when Equations (5) and (6) are applied :

$$uT_x + vT_y = \left(\frac{k_{hnf}}{(\rho C_p)_{hnf}} + \frac{1}{(\rho C_p)_{hnf}} \frac{16\sigma^* T^*}{3k^*} \right) T_{yy} + \frac{Q_0}{(\rho C_p)_{hnf}} (T - T_\infty) + \frac{\mu_{hnf}}{(\rho C_p)_{hnf}} (u_y)^2 + \frac{\sigma_{hnf}}{(\rho C_p)_{hnf}} (B_0 u - E_0)^2 \quad (7)$$

According to the model, the suitable boundary conditions are:

$$\left\{ \begin{array}{l} At \ y = 0, \quad u = 0, N = 0, T = T_w, v = v_w \\ At \ y \rightarrow \infty, \quad u \rightarrow u_e, T \rightarrow T_\infty, N \rightarrow 0 \end{array} \right\} \quad (8)$$

The Spin gradient (γ_{hnf}) expression is:

$$\gamma_{hnf} = j \left(\mu_{hnf} + \frac{K_1}{2} \right) \quad (9)$$

Where σ^* (Stefan-Boltz constant), k^* (mean absorption coefficient), K_1 (vortex viscosity coefficient), $j = \nu_f / c$ (micro inertia constant) and N (a component of micro rotation vector \vec{N} normal).

Tables 1 and 2 provide the numerical expressions for the thermophysical properties of hybrid nanofluids [37–39].

Similarity Transformations

The following is an introduction to the non-dimensional similarity transformations [11, 43]:

Table 1. Base fluid (H_2O) as well as nanoparticle thermophysical characteristics

Physical properties	Fluid phase (f)	Nanoparticles phase (ϕ)	
	H_2O (f)	Silver (ϕ_{Ag})	Alumina ($\phi_{Al_2O_3}$)
Density (ρ), (kg/m^3)	997.1	10,500	3970
Thermal Conductivity (k), (W/mK)	0.613	429	40
Thermal expansion Coefficient (β), ($1/K$)	21×10^{-5}	1.89×10^{-5}	8.5×10^{-6}
Specific heat (C_p), (J/kgK)	4179	235	765
Electric Conductivity (σ), (Ωm) ⁻¹	0.05	6.30×10^7	1×10^{10}
Pr	6.2	-	-

Table 2. Hybrid nanofluid ($Ag-Al_2O_3 / H_2O$) thermophysical properties [40–42]

Properties	Correlations
Dynamic Viscosity	$\frac{\mu_{hnf}}{\mu_f} = (1 - \phi_{Ag} - \phi_{Al_2O_3})^{-2.5}$
Density	$\frac{\rho_{hnf}}{\rho_f} = \phi_{Al_2O_3} \frac{\rho_{Al_2O_3}}{\rho_f} + (-\phi_{Al_2O_3} + 1) \left[(1 - \phi_{Ag}) + \phi_{Ag} \frac{\rho_{Ag}}{\rho_f} \right]$
Electric conductivity	$\frac{\sigma_{hnf}}{\sigma_f} = 1 + \frac{A_a}{A_b}$, Where $\left\{ \begin{array}{l} A_a = 3 \left(\frac{\sigma_{Ag} \phi_{Ag} + \sigma_{Al_2O_3} \phi_{Al_2O_3}}{\sigma_f} \right) - 3(\phi_{Ag} + \phi_{Al_2O_3}), \\ A_b = 2 + \left(\frac{\sigma_{Ag} \phi_{Ag} + \sigma_{Al_2O_3} \phi_{Al_2O_3}}{(\phi_{Ag} + \phi_{Al_2O_3}) \sigma_f} \right) - \left(\frac{\sigma_{Ag} \phi_{Ag} + \sigma_{Al_2O_3} \phi_{Al_2O_3}}{\sigma_f} - (\phi_{Ag} + \phi_{Al_2O_3}) \right) \end{array} \right\}$
Thermal expansion Coefficient	$\frac{(\rho\beta)_{hnf}}{(\rho\beta)_f} = \phi_{Al_2O_3} \frac{(\rho\beta)_{Al_2O_3}}{(\rho\beta)_f} + (-\phi_{Al_2O_3} + 1) \left[(1 - \phi_{Ag}) + \phi_{Ag} \frac{(\rho\beta)_{Ag}}{(\rho\beta)_f} \right]$
Heat capacity	$\frac{(\rho C_p)_{hnf}}{(\rho C_p)_f} = \phi_{Al_2O_3} \frac{(\rho C_p)_{Al_2O_3}}{(\rho C_p)_f} + (1 - \phi_{Al_2O_3}) \left[(1 - \phi_{Ag}) + \phi_{Ag} \frac{(\rho C_p)_{Ag}}{(\rho C_p)_f} \right]$
Thermal conductivity	$\frac{k_{hnf}}{k_f} = \frac{B_a + B_b}{B_a + B_c}$, Where $B_a = \frac{k_{Ag} \phi_{Ag} + k_{Al_2O_3} \phi_{Al_2O_3}}{\phi_{Ag} + \phi_{Al_2O_3}}$, $\left\{ \begin{array}{l} B_b = 2k_f + 2(k_{Ag} \phi_{Ag} + k_{Al_2O_3} \phi_{Al_2O_3}) - 2(\phi_{Ag} + \phi_{Al_2O_3}) k_f, \\ B_c = 2k_f - 2(k_{Ag} \phi_{Ag} + k_{Al_2O_3} \phi_{Al_2O_3}) + (\phi_{Ag} + \phi_{Al_2O_3}) k_f \end{array} \right\}$

$$\begin{aligned} \psi &= (cv_f)^{\frac{1}{2}} xf(\xi), u = \frac{\partial \psi}{\partial y} = cx f'(\xi), v = -\frac{\partial \psi}{\partial x} = -\sqrt{cv_f} f(\xi), \\ \xi &= \sqrt{\frac{c}{v_f}} y, N = cx \sqrt{\frac{c}{v_f}} g(\xi), \theta(\xi) = \frac{T - T_\infty}{T_w - T_\infty}. \end{aligned} \quad (10)$$

Similarly, Equation (10) satisfies Equation (1), whereas the leading Equations. (2), (3), (7), (8), and (9) are reduced to the following dimensionless form:

$$\begin{aligned} &\left(\frac{1 + (1 - \phi_{Ag} - \phi_{Al_2O_3})^{2.5} K}{(1 - \phi_{Ag} - \phi_{Al_2O_3})^{2.5}} \right) f''' + MI_2(1 + E - f') \\ &+ I_1(ff'' + 1 - f'^2) + \lambda I_3\theta + Kg' = 0 \end{aligned} \quad (11)$$

$$\left(\frac{2 + (1 - \phi_{Ag} - \phi_{Al_2O_3})^{2.5} K}{2(1 - \phi_{Ag} - \phi_{Al_2O_3})^{2.5}} \right) g'' - K(2g + f'') + I_1(-f'g + fg') = 0 \quad (12)$$

$$\begin{aligned} (I_5 + Rd)\theta'' + \frac{EcPr}{(1 - \phi_{Ag} - \phi_{Al_2O_3})^{2.5}} f''^2 + I_2EcPrM(f' - E)^2 \\ + PrI_4(\theta'f - f'\theta) + PrQ\theta = 0 \end{aligned} \quad (13)$$

The following boundary conditions are dimensionless:

$$\left\{ \begin{aligned} At \xi = 0, \quad f(\xi) = S, f'(\xi) = 0, \theta(\xi) = 1, g(\xi) = 0, \\ As \xi \rightarrow \infty, \quad f'(\xi) \rightarrow 1, g(\xi) \rightarrow 0, \theta(\xi) \rightarrow 0. \end{aligned} \right\} \quad (14)$$

Here, ξ (dimensionless similarity variable), $f(\xi)$ (dimensionless stream function), $f'(\xi)$ (dimensionless velocity profile), $\theta(\xi)$ (non-dimensional temperature), $g(\xi)$ (dimensionless micro-rotation velocity profile), $Gr_x = g\beta_f(T_w - T_\infty)/\nu_f^2$ (Grashof number), $E = E_0 / B_0u_e$ (Electric field factor), $Ec = u_e^2(x)/(c_p)_f(T_w - T_\infty)$ (Eckert number), $(\mu C_p)_f/k_f$ (Prandtl number), $K = K1/\mu_f$ (Micropolar parameter), $M = \sigma_f B_0^2/\rho_f c$ (Magnetic factor), $\lambda = Gr_x/Re_x^2$ (Mixed convection parameter), $Rd = 16\sigma^*T_\infty^3/3k_f k$ (Thermal radiation factor), $S = -v_w/\sqrt{cv_f}$ (Suction/injection parameter), $Re_x = u_e(x)x/\nu_f$ (Reynolds number), $Q = Q_0/c(\rho C_p)_f$ (Heat source /sink factor), $I_1 = \rho_{hnf}/\rho_f$, $I_2 = \sigma_{hnf}/\sigma_f$, $I_3 = (\rho\beta)_{hnf}/(\rho\beta)_f$, $I_4 = (\rho C_p)_{hnf}/(\rho C_p)_f$ and $I_5 = k_{hnf}/k_f$.

Important quantities

The skin friction coefficient (C_f) and the Nusselt number (Nu) are crucial to this problem, and they are defined mathematically as follows [11, 44]:

$$C_{fx} = \frac{1}{P_{hnf} u_e^2(x)} \left[(\mu_{hnf} + K_1) u_y + K_1 N \right]_{y=0} \quad (15)$$

$$Nu_x = - \left[\left(k_{hnf} T_y + \frac{16\sigma^*}{3k^*} T^3 T_y \right) \frac{x}{k_f (T_w - T_\infty)} \right]_{y=0} \quad (16)$$

By using Eq. (10), the preceding equations can be simplified to:

$$C_f = \frac{1}{I_1} \left[\frac{1 + (1 - \phi_{Ag} - \phi_{Al_2O_3}) K}{(1 - \phi_{Ag} - \phi_{Al_2O_3})} \right] f''(0) \quad (17)$$

$$Nu = -(I_5 + Rd)\theta'(0) \quad (18)$$

Where $C_f = C_{fx} (Re_x)^{0.5}$ and $Nu = Nu_x (Re_x)^{-0.5}$

Solution Methodology

The system of Equations (11)-(13) is nonlinear and cannot be resolved using analytical methods. As a result, numerical methods have to be used to compute the aforementioned ODEs. As a result, in the present research, the inbuilt function `bvp4c` in MATLAB software is employed to solve the provided model. The acceptable threshold for convergence conditions was set at 10^{-6} . The skin friction coefficient and Nusselt numbers were determined through numerical computations. For the linearization, Equations (11)-(13) were used to do the linearization, and Equation 14 was used to specify the boundaries. The following assumptions were employed in favor of the system solution.

$$\left\{ \begin{aligned} f &= y(1), f' = y(2), f'' = y(3), g = y(4) \\ g' &= y(5), \theta = y(6), \theta' = y(7) \end{aligned} \right\} \quad (19)$$

Inserting Equation 19 into Equations (11)-(13) the resulting new systems are:

$$\begin{aligned} f''' &= \frac{1}{\left(\frac{1 + (1 - \phi_{Ag} - \phi_{Al_2O_3})^{2.5} K}{(1 - \phi_{Ag} - \phi_{Al_2O_3})^{2.5}} \right)} \left(-I_1(1 + ff'' - f'^2) \right. \\ &\left. - Kg' - MI_2(E - f' + 1) - \lambda I_3\theta \right) \end{aligned} \quad (20)$$

$$g'' = \frac{1}{\left(\frac{2 + (1 - \phi_{Ag} - \phi_{Al_2O_3})^{2.5} K}{2(1 - \phi_{Ag} - \phi_{Al_2O_3})^{2.5}} \right)} \left(-I_1(g'f - gf') + K(f'' + 2g) \right) \quad (21)$$

$$\begin{aligned} \theta'' &= \frac{1}{(I_5 + Rd)} \left(-\frac{EcPr}{(1 - \phi_{Ag} - \phi_{Al_2O_3})^{2.5}} f''^2 - I_2EcPrM(f' - E)^2 \right. \\ &\left. - PrI_4(\theta'f - f'\theta) - PrQ\theta \right) \end{aligned} \quad (22)$$

The boundary conditions that relate to them are:

$$\left\{ \begin{aligned} y_1(0) &= s, y_2(0) = 0, y_4(0) = 0, y_6(0) = 1 \quad \text{at } \xi = 0 \\ y_2(\infty) &= 1, y_4(\infty) = 0, y_6(\infty) = 0 \quad \text{at } \xi \rightarrow \infty \end{aligned} \right\} \quad (23)$$

We look at how parameters change across multiple graphs. using Equations (20)-(22) and the boundary condition (23).

RESULTS AND DISCUSSION

The objective of this part is to go over how different embedding factors influence the temperature, micro rotation, and velocity profiles as seen in Figures 2-15, which are

all related to the aforementioned flow problems. It should be noted that during the explanation of outcomes using pictorial views, we utilized constant mathematical values for significant parameters such as $\phi_{Ag} = \phi_{Al_2O_3} = 4\%$, $\lambda = 0.5$, $Pr = 6.2$, $Q = 0.1$, $Rd = 4$, $E = 0.1$ and $S = 0.5$ [11]. The outcomes of the present study are compared to those of prior works in Tables 3 and 4. Full agreement with the research of Aman et al. [45] and Lok et al. [46] is revealed. Table 5 displays the outcomes of C_f and Nu across different E values. It's clear that higher E values correlate with increased C_f and Nu rates. This phenomenon is attributed to the induction of electrokinetic phenomena by electric fields, such as electroosmosis and electrophoresis. These phenomena enhance fluid motion and heat transfer near the surface, resulting in elevated skin friction and Nusselt values. In Figure 2, we see how the velocity ($f'(\xi)$) of a ($Ag-Al_2O_3 / H_2O$) hybrid nanofluid changes as the micropolar parameter (K) is increased. Here We noticed that as K increased, $f'(\xi)$ decreased, which is consistent with a result produced by Algehyne et al. [44]. The reason for this is that a rise in K induces the momentum layer's width to decrease at the boundaries, leading to a decrease in fluid motion. The result of K on $\theta(\xi)$ of the hybrid nanofluid ($Ag-Al_2O_3 / H_2O$) is displayed in Figure 3. From this, we note that the increasing K substantially elevates the temperature. Because the effects of heating within the thermal boundary layer get stronger at higher K values. Figure 4 shows how the micro-polar parameter K of the hybrid nanofluid ($Ag-Al_2O_3 / H_2O$) flow affects the $g(\xi)$. From this, it can be shown that a rise in K lowers $g(\xi)$. The reason for this is the potential for micro-motion events near a flat surface to be weaker. The behavior of $f'(\xi)$ for increasing readings of M within a hybrid nanofluid ($Ag-Al_2O_3 / H_2O$) flow is seen in Figure 5. Here, we found that raising M significantly raises the $f'(\xi)$, Algehyne et al. [44] and Uddin et al. [47] established an equivalent conclusion. Because a boundary layer for the flow of hybrid nanofluids becomes smaller as the magnetic field becomes stronger because of the Lorentz force regarding the magnetic field. Magnetic lines of force travel over the plate at free stream velocity. The magnetic field provides an impulsion to the fluid that is being slowed down by the viscous force, counteracting the viscous effect. Consequently, as the value of M grows, the velocity of the hybrid nanofluid flow under consideration also increases and converges towards the boundary. Therefore, an enhancement in M raises the $f'(\xi)$.

The effect of M on $\theta(\xi)$ towards the hybrid nanofluid is shown in Figure 6. The observed phenomenon implies that a rise in M causes a significant increase in $\theta(\xi)$. This is because the rising magnetic field causes the thicker thermal boundary layer of the hybrid nanofluid flow to rise. Heat transfer to the wall is decreased by the functional magnetic field, which heats the fluid as a result of electromagnetic work, causing temperature profiles to rise. The effect of M on the hybrid nanofluid ($Ag-Al_2O_3 / H_2O$) flows $g(\xi)$ is seen in Figure 7. Here, we saw that the microrotation velocity profile decreases with an interval of $0 < x < 0.6$ magnetic

Table 3. Comparison of $f''(0)$ at distinct values of Pr for the case where $\lambda = 1$ and a range of other parameters are all set to zero

Pr	Aman et al. [45]	Lok et al. [46]	Current findings
0.7	1.7063	1.7063	1.706215
1	1.6754	-	1.675424
7	1.5179	1.5179	1.517915
10	1.4928	-	1.492841
20	1.4485	1.4485	1.448486
40	1.4101	1.4101	1.410060
50	1.3989	-	1.398933
60	1.3903	1.3903	1.390377
80	1.3774	1.3774	1.377395
100	1.3680	1.3680	1.368037

Table 4. Comparison of $-\theta(0)$ at various values of Pr for the case where $\lambda = 1$ and a range of other parameters are all set to zero

Pr	Aman et al. [45]	Lok et al. [46]	Current findings
0.7	0.7641	0.7641	0.764178
1	0.8708	-	0.870790
7	1.7224	1.7224	1.722383
10	1.9446	-	1.944619
20	2.4576	2.4576	2.457592
40	3.1011	3.1011	3.101096
50	3.3415	-	3.341460
60	3.5514	3.5514	3.551409
80	3.9095	3.9095	3.909484
100	4.2116	4.2116	4.211649

Table 5. Presents the numerical data of $f''(0)$ and $-\theta'(0)$ corresponding to different E values

E	$f''(0)$	$-\theta'(0)$
0.2	1.969033	5.642665
0.4	2.033144	5.724474
0.6	2.097130	5.776319
0.8	2.160982	5.799067

factor near the flat surface and increases with an interval of $0.6 < x < 4$ magnetic parameters farther from the flat surface. Figure 8 reveals the effect of E on $f'(\xi)$. Here, we observed that a larger electric field (E) enhances the $f'(\xi)$, and Devi and Niranjana [48] established a similar conclusion. Lorentz force, the result of the interaction between magnetic and electric fields, is observed here to reduce fluid velocity. However, in this investigation, the momentum

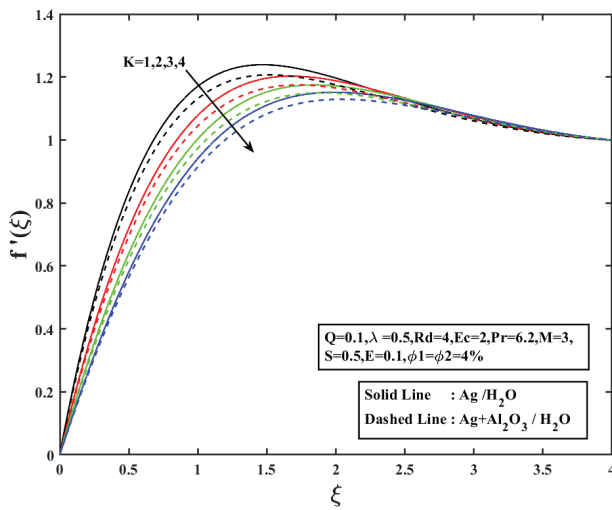


Figure 2. Effect of K on $f'(\xi)$.

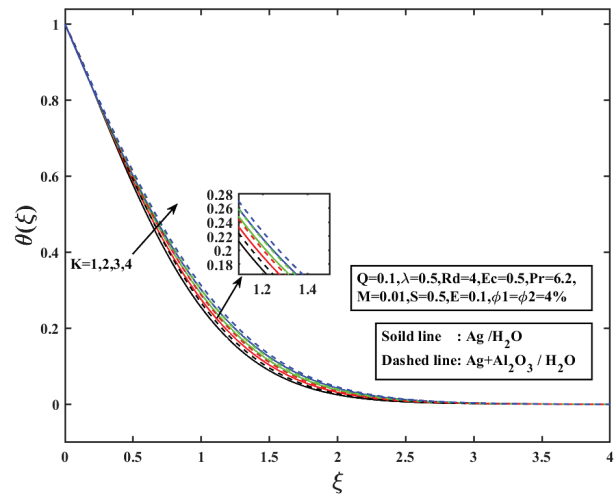


Figure 3. Effect of K on $\theta(\xi)$.

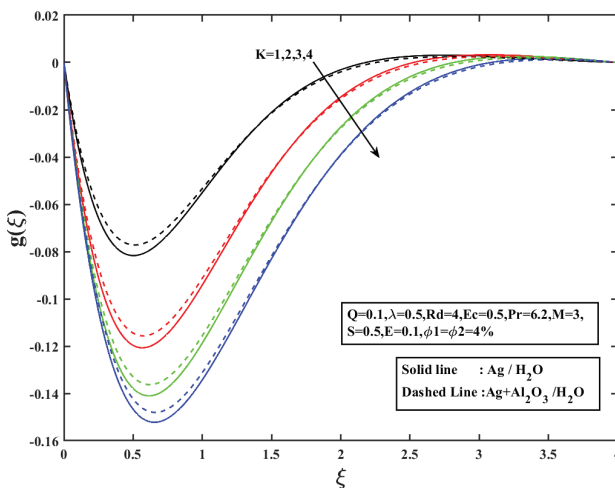


Figure 4. Effect of K on $g(\xi)$.

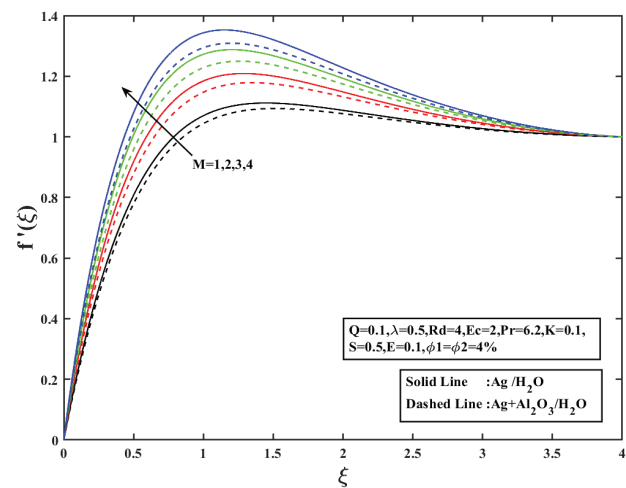


Figure 5. Effect of M on $f'(\xi)$.

barrier layer thickness is more important than the Lorentz force because of the surface flow with a stagnation point. When the strength of the electric field is raised, a thicker momentum barrier layer develops. In Figure 9, we see how changing E affects $\theta(\xi)$ in the hybrid nanofluid. It is clear that as E is raised, the $\theta(\xi)$ is reduced and similar findings were achieved by Devi and Niranjana [48]. This is because, as E increases in magnitude, the Lorentz force decelerates the body force, resulting in a thermally smaller boundary layer. As shown in Figure 10, a hybrid nanofluid's micro-rotation profile is affected by E. In this case, a double impact is seen as the E parameter is raised, confirmed by previous work of Shah et al. [16]. At close to the flat surface, the electric factor reduces $g(\xi)$, as one moves out from the surface of influence, the effect grows also for the higher values of

E produce fast ionization in micropolar hybrid nanofluid and hence the motion of hybrid nanoparticle also rises. The effect of λ on $f'(\xi)$ is shown in Figure 11. As the value of λ increases, it can be seen that $f'(\xi)$ also grows. This is because buoyancy-induced flow is superimposed over the externally-forced convection flow. As a result, the velocity profile rises with increasing λ . Figure 12 shows that, just like with magnetic and electric field effects, greater values of λ have a double influence on $g(\xi)$. It is evident that the $g(\xi)$ profile decreases from $0 < \xi < 0.4$ and that the size of the momentum boundary layer rises from $0.4 < \xi < 3$ therefore, the $g(\xi)$ of the fluid grows. Figure 13 displays the impact of Rd on $\theta(\xi)$. It is observed that the temperature profile grows as the levels of Rd increase. This is because, as a matter of physics, the presence of heat flux induces a rise in temperature

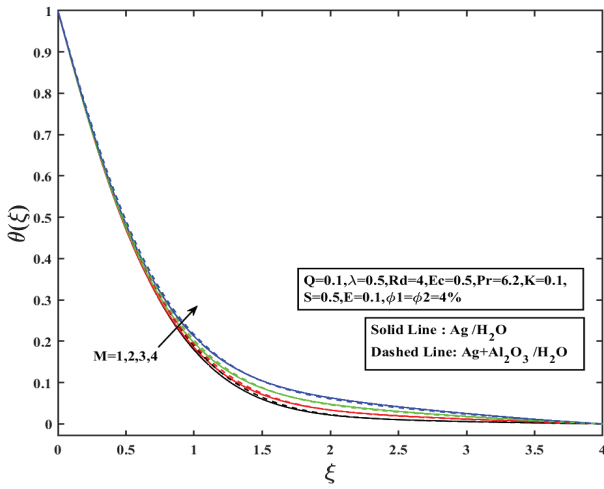


Figure 6. Effect of M on $\theta(\xi)$.

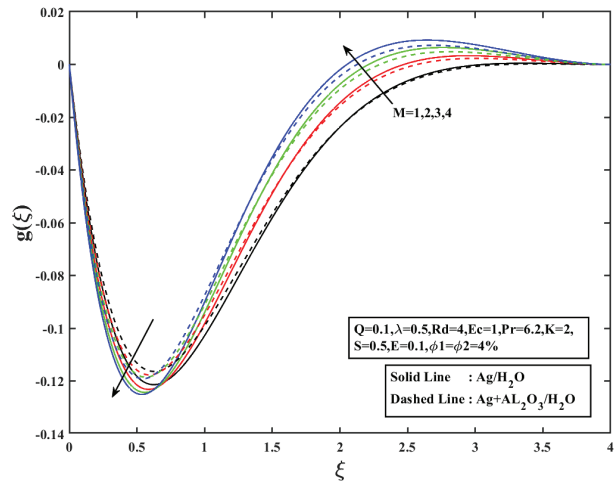


Figure 7. Effect of M on $g(\xi)$.

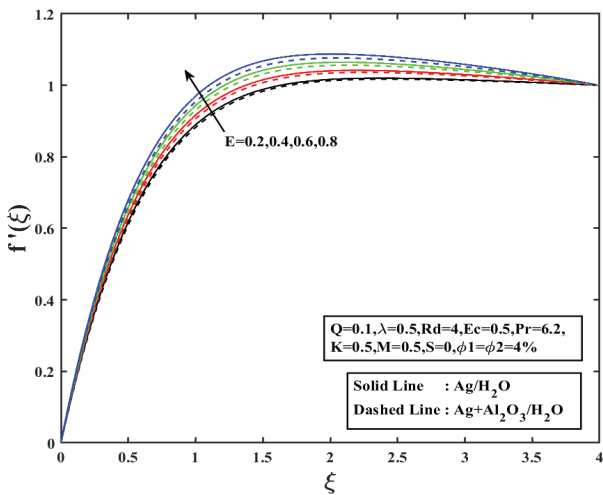


Figure 8. Effect of E on $f'(\xi)$.

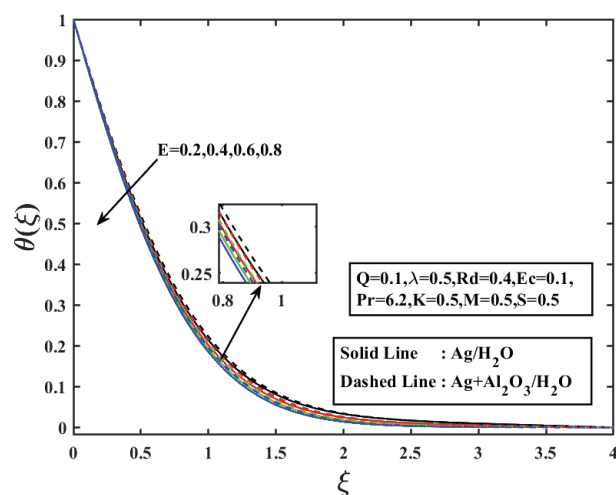


Figure 9. Effect of E on $\theta(\xi)$.

over the entire flow region's thermal boundary layer. This is because, as the Rosseland diffusion application gets warmer, the temperature profile also rises. In Figure 14, we can observe the impact of Ec on $\theta(\xi)$. Here, we see that the temperature rises along with the Ec values due to the heat produced by the fluid motion. Since the Ec is equal to the sum of the specific enthalpy released by the kinetic energy of the fluid, and how it interacts with the wall, an increase in Ec indicates that work has been performed in response to the stresses of the viscous fluid, which convert the fluid's kinetic energy into internal energy. Figure 15 illustrates how Q influences $\theta(\xi)$. In general, a higher Q results in a hotter overall distribution. When Q is increased, the liquid's temperature rises because the particles in the liquid have a greater amount of intrinsic energy.

In engineering, the calculations of shear stress (skin friction) and plate thermal transfer are of particular interest. Since shear stress correlates so closely with heat transfer coefficients. It is very important to understand how heat is transferred. In most technical situations, a rise in shear stress is inconvenient. Also, while the increased heat transfer can be used to one's advantage in some contexts, such as heat exchangers, should be avoided in others, such as gas turbines. Figures 16–21 display the results for the C_f and the Nu for a range of E and Rd values since the volume fraction ϕ_1 and ϕ_2 was increased. It can be seen in Figures 16 and 17 show the heat transfer rate is changed by the electric field and the volume fraction ϕ_1 and ϕ_2 . It appears that when E increases, the heat transfer rate peaks between $0.6 < E < 1.2$ and that at higher levels of E , the Nu is lowered. Raising the volume fraction ϕ_1 and ϕ_2 causes a drastic decrease in the

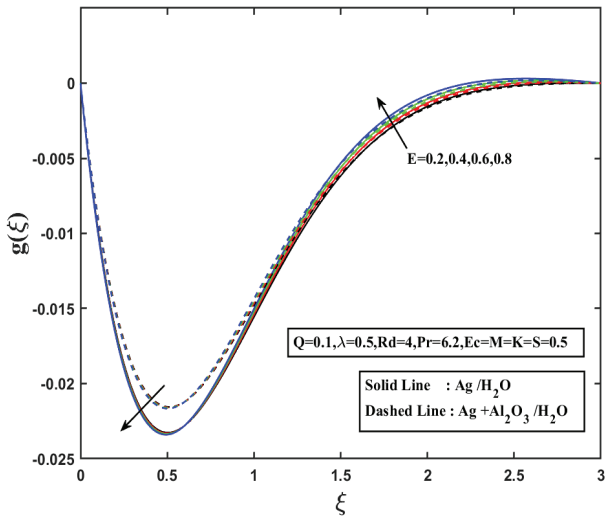


Figure 10. Effect of E on $g(\xi)$.

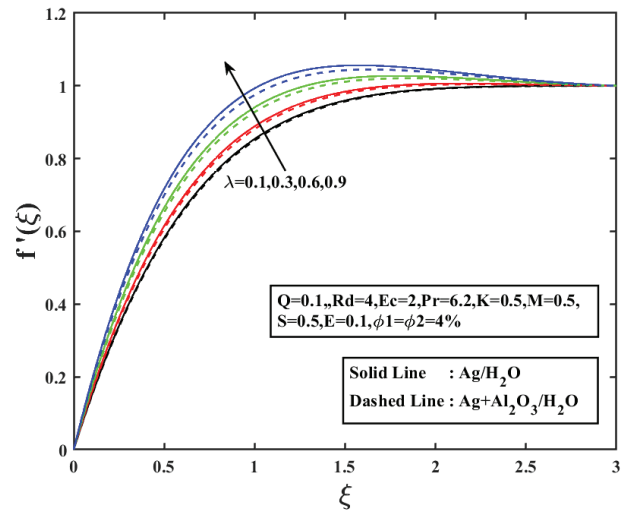


Figure 11. Effect of λ on $f'(\xi)$.

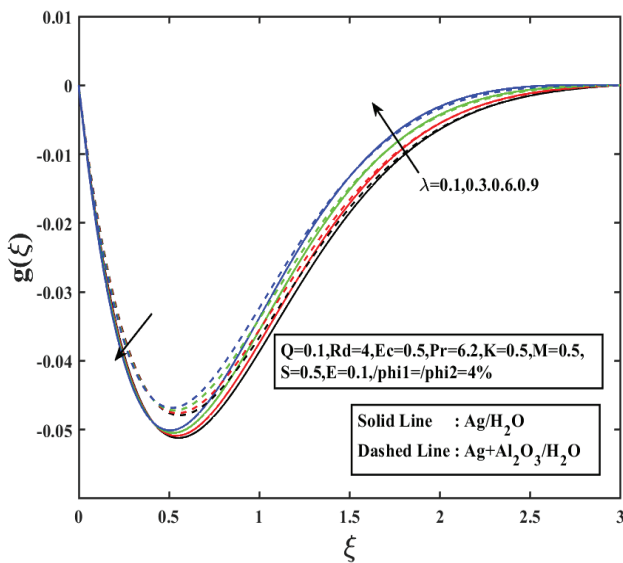


Figure 12. Effect of λ on $g(\xi)$.

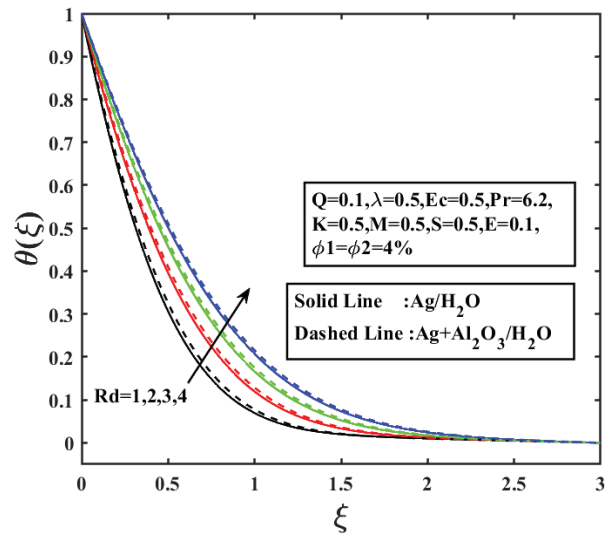


Figure 13. Effect of Rd on $\theta(\xi)$.

heat transfer rate. From this, we concluded that a minimal Nu requires a volume proportion ϕ_1 , ϕ_2 , and E to be large. To achieve maximum Nu , the volume fractions ϕ_1 and ϕ_2 should be kept as low as possible, with E falling between $0.6 < E < 1.2$. Because of the hybrid nanofluid's enhanced heat transmission performance due to its increased thermal conduction, this phenomenon has been seen. Figures 18 and 19 show how the skin friction changes as a function of the electric field and the volume fractions ϕ_1 and ϕ_2 . The skin friction coefficient rises with increasing electric field strength, as it declines the volume fractions ϕ_1 and ϕ_2 grows larger. Based on these results, we deduced that the values of ϕ_1 and ϕ_2 should be greater and E should be lower

to achieve the least of C_f , but the reverse trend is followed to get the greatest of skin friction. Figures 20 and 21 show the effect that Rd has on Nu when the values of ϕ_1 and ϕ_2 are increased. Here, we found that ϕ_1 and ϕ_2 don't contribute much to heat transmission, and that Rd values that are lower reduced the heat transfer rate regardless of ϕ_1 and ϕ_2 .

We find that the Nu increases with increasing Rd, independent of the values of ϕ_1 and ϕ_2 because as Rd values increase, the thermal resistance between the surface and the fluid decreases, resulting in increased heat transfer effectiveness. This decreased thermal resistance results in higher Nusselt numbers, as heat is transferred more effectively from the surface to the fluid.

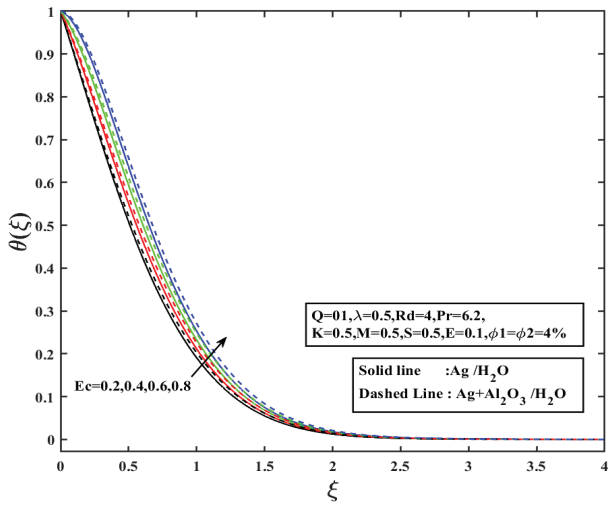


Figure 14. Effect of Ec on $\theta(\xi)$.

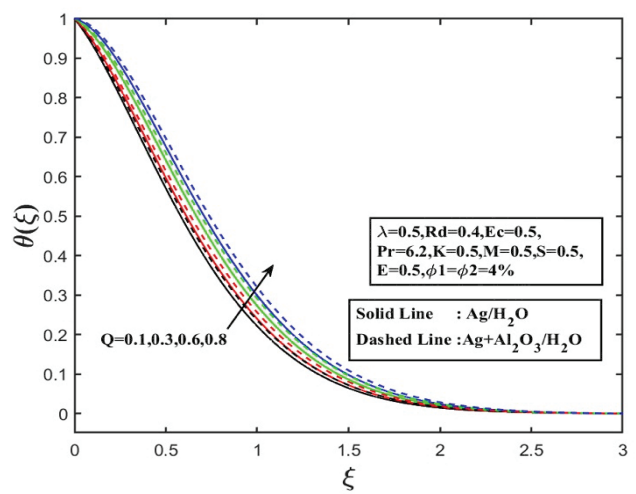


Figure 15. Effect of Q on $\theta(\xi)$.

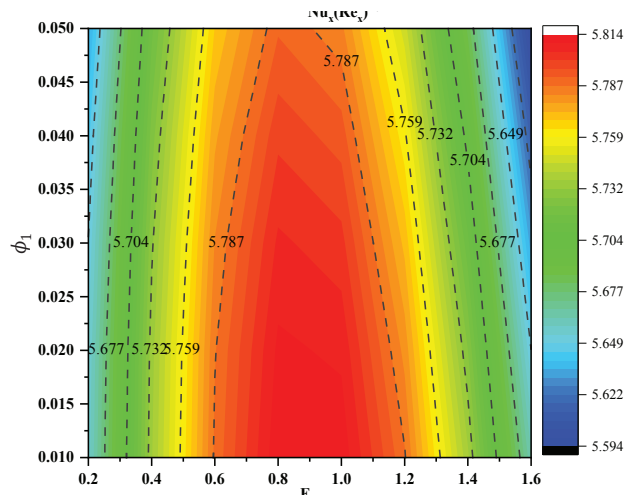


Figure 16. Effect of ϕ_1 and E on $Nu_x(Re_x)^{-0.5}$.

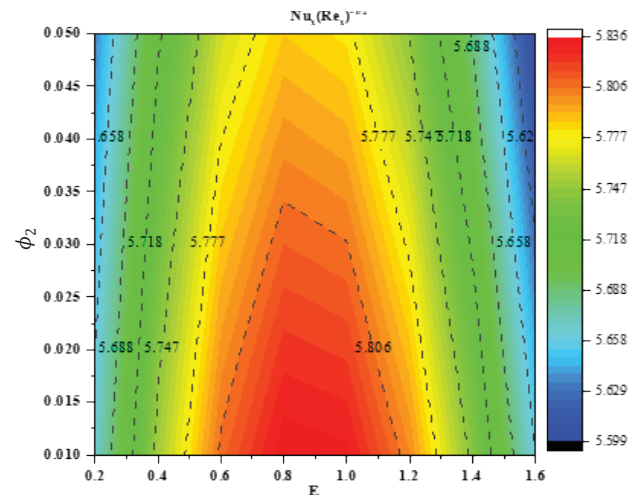


Figure 17. Effect of ϕ_2 and E on $Nu_x(Re_x)^{-0.5}$.

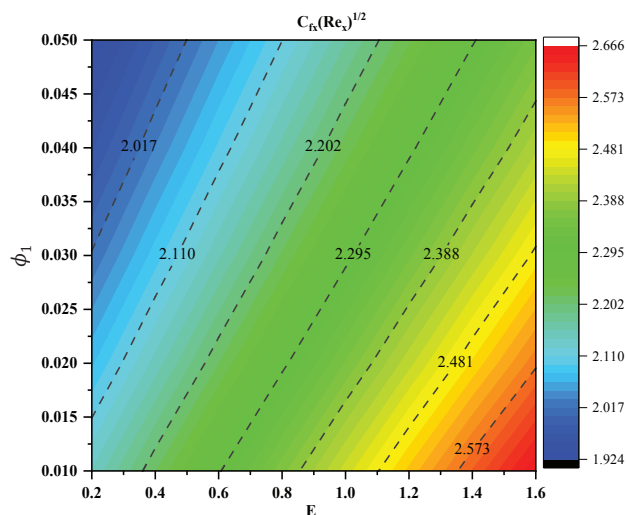


Figure 18. Effect of ϕ_1 and E on $C_{fx}(Re_x)^{0.5}$.

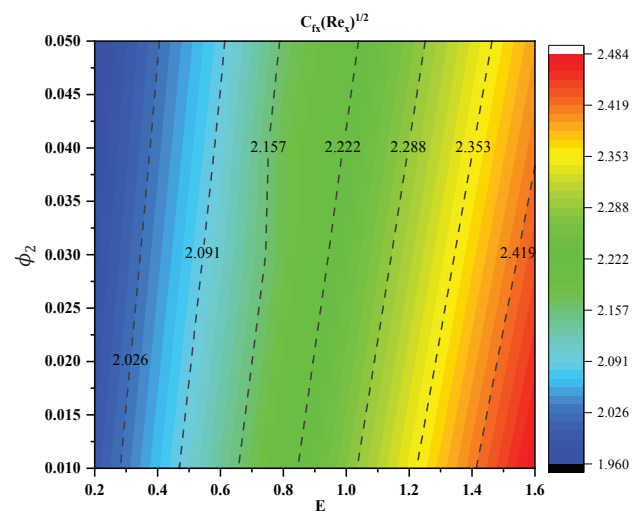


Figure 19. Effect of ϕ_2 and E on $C_{fx}(Re_x)^{0.5}$.

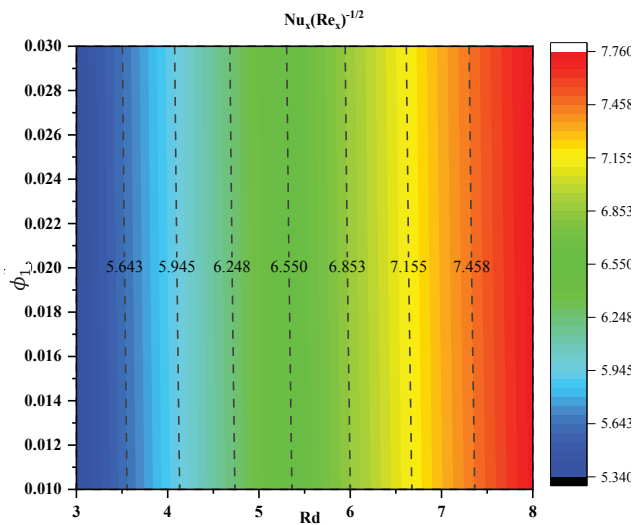


Figure 20. Effect of ϕ_1 and Rd on $Nu_x(Re_x)^{-0.5}$.

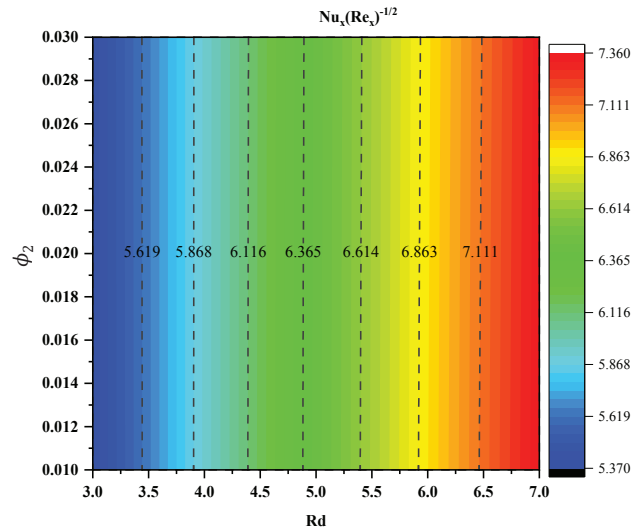


Figure 21. Effect of ϕ_2 and Rd on $Nu_x(Re_x)^{-0.5}$.

CONCLUSION

The current study looks into electrically conducted MHD micropolar hybrid nanofluid passing via a flat surface. The plate is vertically positioned in a permeable material having suction as well as injection actions. Water with ($Ag-Al_2O_3$) hybrid nanoparticles suspended in it forms the enclosure's fluid. A suitable variables transformation can be used to convert the nonlinear system of PDEs into dimensionless form. The built-in function `bvp4c` in MATLAB software can be used to solve the problem numerically. The outcomes of these numeric calculations are illustrated graphically and discussed in detail for a range of input values. The following is a summary of the main points:

- As E rises, a dual influence is observed on the micro rotational velocity profile and increases on the velocity profile.
- The decreasing significance of the velocity profile and micro rotational velocity profile can be attributed to the growing value of K .
- The thermal flow behaviour improves for larger K , M , Rd , Ec , and Q values and deteriorates with the electric component.
- Increasing mixed convection parameter values raises velocity profile but has a double effect on microrotational distribution.
- The minimum heat transfer rate requires a volume fraction ϕ_1 , ϕ_2 and E to be large. To achieve maximum heat transfer rate, the volume fractions ϕ_1 and ϕ_2 should be kept as low as possible, with E falling between $0.6 < E < 1.2$.
- The values of ϕ_1 and ϕ_2 should be greater and E should be lower to achieve the least of skin friction, but the reverse trend is followed to get the greatest of skin friction.
- The higher Rd values cause a corresponding increase in heat transfer rate.

- The hybrid nanofluids have a greater thermal flow rate than either nanofluids or base fluids.

Many disciplines can benefit from this study. Aerospace engineers can use it to model the behaviour of electrically conducting flows when exposed to electromagnetic fields. Engineers in the water treatment industry can use it to control electromagnetic fields on a small scale in desalination membranes and heat exchangers also with the use of electric field effects, dielectric heating systems can quickly and evenly heat food products. Improved heat transfer efficiency by combining the effects of electric fields, thermal radiation, and micropolar fluid behaviour allows for energy-efficient processing without affecting the nutritional value as well as sensory attributes of the food. Finally, medical professionals can use it for diagnostic imaging (Magnetic Resonance Imaging), malaria treatment, and uterine tumours.

NOMENCLATURE

B_0	Strength of magnetic field (<i>Telsa</i>)
C_f	Skin Friction Coefficient (dimensionless)
C_p	Specific heat capacity (Joules per kilogram per degree Celsius)
E	Electric field factor (dimensionless)
Ec	Eckert number (dimensionless)
f	Dimensionless stream function
$f'(\xi)$	Dimensionless velocity profile
Gr_x	Grashof number (dimensionless)
g	Gravitational acceleration (Meters per second squared)
$g(\xi)$	Dimensionless micro-rotational velocity profile
j	Micro inertia constant (Kilograms per meter)
K	Micropolar parameter (dimensionless)
k	Thermal conductivity (Watts per meter per degree)
K_1	Vortex viscosity coefficient (Pascals seconds)

k^*	Mean absorption coefficient (Inverse meters)
M	Magnetic field parameter (dimensionless)
Nu	Nusselt number (dimensionless)
N	A component of micro rotation vector \vec{N} normal (dimensionless)
Pr	Prandtl number (dimensionless)
Q	Heat source/sink parameter (dimensionless)
q_r	Radiant heat flux (Watts per square meter)
Rd	Thermal radiation parameter (dimensionless)
Re_x	Reynolds number (dimensionless)
S	Suction/injection parameter (dimensionless)
T	Temperature (Degrees Celsius)
u_e	Free stream velocity (Meters per second)
u, v	Velocity components along the x and y -axis (Meters per second)

Greek symbols

λ	Mixed convection (dimensionless)
β	Coefficient of thermal expansion (Inverse Kelvin)
ϕ_{Ag}	The silver nanoparticle volume fraction
$\phi_{Al_2O_3}$	Alumina nanoparticle volume fraction
θ	Dimensionless temperature
ξ	Similarity variable (dimensionless)
μ	Dynamic viscosity (Pascal seconds)
ρ	Density (Kilograms per cubic meter)
γ	Spin gradient (Inverse meters)
σ^*	Stefan-Boltzmann constant (Watts per square meter per Kelvin to the fourth power)
ν	Kinematic viscosity (Square meters per second)
σ	Electric conductivity (Siemens per meter)
$\theta(\xi)$	Dimensionless temperature profile
Ψ	Stream function (dimensionless)

Subscripts

W	At wall
∞	At free stream

Abbreviations

MHD	Magnetohydrodynamic
ODE's	Ordinary Differential Equations
PDE's	Partial Differential Equations
hnf	hybrid nanofluid
nf	nanofluid
f	Fluid (Water)

AUTHORS CONTRIBUTION

All authors contributed equally to the writing of this paper. All authors read and approved the final manuscript.

DATA AVAILABILITY STATEMENT

The authors confirm that the data that supports the findings of this study are available within the article. Raw data that support the finding of this study are available from the corresponding author, upon reasonable request.

CONFLICT OF INTEREST

The authors declare that they have no known competing financial interests reported in this paper.

ETHICS

There are no ethical issues with the publication of this manuscript.

ACKNOWLEDGEMENTS

We would like to extend our sincere appreciation to the reviewers for their constructive and helpful suggestions to improve the contents of the manuscripts. We did not receive any financial support from any agencies.

REFERENCES

- [1] Jamil F, Ali HM. Applications of hybrid nanofluids in different fields. In: Ali HM, ed. Hybrid Nanofluids for Convection Heat Transfer. Cambridge, MA: Academic Press; 2020. [CrossRef]
- [2] Suneetha S, Subbarayudu K, Bala Anki Reddy P. Hybrid nanofluids development and benefits: A comprehensive review. J Therm Engineer 2022;8:445-455. [CrossRef]
- [3] Chu YM, Khan MI, Abbas T, Sidi MO, Alharbi KAM, Alqsair UF, et al. Radiative thermal analysis for four types of hybrid nanoparticles subject to non-uniform heat source: Keller box numerical approach. Case Stud Therm Engineer 2022;40:102474. [CrossRef]
- [4] Khan MR, Pan K, Khan AU, Nadeem S. Dual solutions for mixed convection flow of $SiO_2-Al_2O_3$ /water hybrid nanofluid near the stagnation point over a curved surface. Phys A Stat Mech Appl 2019;547:123959.
- [5] Kayalvizhi J, Vijaya Kumar AG. Entropy analysis of EMHD hybrid nanofluid stagnation point flow over a porous stretching sheet with melting heat transfer in the presence of thermal radiation. Energies 2022;15:8317. [CrossRef]
- [6] Mandal G. A numerical study of Ag – M gO / water hybrid micropolar nano uid ow with effects of quadratic thermal radiant energy along an exponentially contracting permeable Riga surface: Stability and Entropy optimization. Research Square 17 Aug 2023. Doi: <https://doi.org/10.21203/rs.3.rs-3260581/v1>. [Preprint] [CrossRef]
- [7] Roy S, Asirvatham LG, Kunhappan D, Cephas E, Wongwises S. Heat transfer performance of Silver/ Water nanofluid in a solar flat-plate collector. J Therm Engineer 2015;1:104-112. [CrossRef]
- [8] Paul A, Nath JM, Das TK. An investigation of the MHD Cu- Al_2O_3 /H $_2$ O hybrid-nanofluid in a porous medium across a vertically stretching cylinder incorporating thermal stratification impact. J Therm Engineer 2023;9:799-810. [CrossRef]

- [9] Singh U, Pandey H, Gupta NK. An exploratory review on heat transfer mechanisms in nanofluid based heat pipes. *J Therm Engineer* 2023;9:1339-1355. [CrossRef]
- [10] Eringen AC. Irreversible thermodynamics and continuum mechanics. *Phys Rev A* 1960;117:1174-1183. [CrossRef]
- [11] Lone SA, Alyami MA, Saeed A, Dawar A, Kumam P, Kumam W. MHD micropolar hybrid nanofluid flow over a flat surface subject to mixed convection and thermal radiation. *Sci Rep* 2022;12:1-14. [CrossRef]
- [12] Zaib A, Khan U, Shah Z, Kumam P. Optimization of entropy generation in flow of micropolar mixed convective magnetite (Fe_3O_4) ferroparticle over a vertical plate. *Alexandria Engineer J* 2019;58:1461-1470. [CrossRef]
- [13] Tripathi D, Prakash J, Tiwari AK, Ellahi R. Thermal, microrotation, electromagnetic field and nanoparticle shape effects on Cu-CuO / blood flow in microvascular vessels. *Microvas Res* 2020;132:104065. [CrossRef]
- [14] Bansal P, Chattopadhyay AK, Agrawal VP. Linear stability analysis of hydrodynamic journal bearings with a flexible liner and micropolar lubrication. *Tribol Transac* 2015;58:316-326. [CrossRef]
- [15] Tanuja TN, Kavitha L, Varma AVK, Khan U, Sherif ESM, Hassan AM, et al. Flow and heat transfer analysis on micropolar fluid through a porous medium between a clear and $\text{Al}_2\text{O}_3\text{-Cu}/\text{H}_2\text{O}$ in conducting field. *Front Mater* 2023;10:1216757. [CrossRef]
- [16] Shah Z, Islam S, Gul T, Bonyah E, Altaf Khan M. The electrical MHD and Hall current impact on micropolar nanofluid flow between rotating parallel plates. *Results Phys* 2018;9:1201-1214. [CrossRef]
- [17] Khan U, Zaib A, Abu Bakar S, Ishak A. Stagnation-point flow of a hybrid nanoliquid over a non-isothermal stretching/shrinking sheet with characteristics of inertial and microstructure. *Case Stud Therm Engineer* 2021;26:101150. [CrossRef]
- [18] Ram SR, Bandaru S, Salawu AO, Mohammed SP. A numerical study of radiation effects of an unsteady micropolar fluid through porous medium with MHD boundary layer flow near the stagnation point towards a shrinking surface. *Research Square* 21 Feb 2023. Doi: <https://doi.org/10.21203/rs.3.rs-2603496/v1>. [Preprint] [CrossRef]
- [19] Roja P, Reddy TS, Ibrahim SM, Parvathi M, Dharmiah G, Lorenzini G. Magnetic field influence on thermophoretic micropolar fluid flow over an inclined permeable surface: A numerical study. *J Appl Comp Mech* 2024;10:369-382.
- [20] Alqahtani AM, Zeeshan KW, Amina ASA, El-Wahed KHA. Stability of magnetohydrodynamics free convective micropolar thermal liquid movement over an exponentially extended curved surface. *Heliyon* 2023;9:e21807. [CrossRef]
- [21] Mollamahdi M, Abbaszadeh M, Sheikhzadeh GA. Analytical study of $\text{Al}_2\text{O}_3\text{-Cu}/$ water micropolar hybrid nanofluid in a porous channel with expanding / contracting walls in the presence of magnetic field. *ScientiaIranica* 2018;25:208-220. [CrossRef]
- [22] Jawad M, Khan Z, Bonyah E, Jan R. Analysis of hybrid nanofluid stagnation point flow over a stretching surface with melting heat transfer. *Math Problems Engineer* 2022;9469164. [CrossRef]
- [23] Joule's 1840 manuscript on the production of heat by voltaic electricity. *Notes and Records* 2020;76(1):117-153. Available at: doi:10.1098/rsnr.2020.0027. [CrossRef]
- [24] Khan SA, Khan MI, Alsallami SAM, Alhazmi SE, Alharbi FM, El-Zahar ER. Irreversibility analysis in hydromagnetic flow of Newtonian fluid with Joule heating: Darcy-Forchheimer model. *J Petrol Sci Engineer* 2022;212:110206. [CrossRef]
- [25] Saeed A, Alsubie A, Kumam P, Nasir S, Gul T. Blood based hybrid nanofluid flow together with electromagnetic field and couple stresses. *Sci Rep* 2021;12865. [CrossRef]
- [26] Shamshuddin MD, Mishra SR, Bég OA, Kadir A. Unsteady reactive magnetic radiative micropolar flow, heat and mass transfer from an inclined plate with Joule heating: A model for magnetic polymer processing. *Proc Inst Mech Engineer C: J Mech Engineer Sci* 2019;233:1246-1261. [CrossRef]
- [27] Pramanik S. Casson fluid flow and heat transfer past an exponentially porous stretching surface in presence of thermal radiation. *Ain Shams Engineer J* 2014;5:205-212. [CrossRef]
- [28] Hassan AR, Fenuga OJ. The effects of thermal radiation on the flow of a reactive hydromagnetic heat generating couple stress fluid through a porous channel. *SN Appl Sci* 2019;1:1-10. [CrossRef]
- [29] Reddy YD, Shankar Goud B. Comprehensive analysis of thermal radiation impact on an unsteady MHD nanofluid flow across an infinite vertical flat plate with ramped temperature with heat consumption. *Results Engineer* 2023;17:100796. [CrossRef]
- [30] Srilatha P, Hassan AM, Goud BS, Kumar ER. Mathematical Study of MHD micropolar fluid flow with radiation and dissipative impacts over a permeable stretching sheet: Slip effects phenomena. *Front Heat Mass Transf* 2023;21:539-562. [CrossRef]
- [31] Jakeer S, Bala Anki Reddy P. Entropy generation on EMHD stagnation point flow of hybrid nanofluid over a stretching sheet: Homotopy perturbation solution. *Phys Scr* 2020;95:125203. [CrossRef]
- [32] Abbas SZ, Khan WA, Gulzar MM, Hayt T, Waqas M, Asghar Z. Magnetic field influence in three-dimensional rotating micropolar nanoliquid with convective conditions. *Comp Meth Prog Biomed* 2020;189:105324. [CrossRef]

- [33] Hosseinzadeh K, Roghani S, Asadi A, Mogharrebi A, Ganji DD. Investigation of micropolar hybrid ferrofluid flow over a vertical plate by considering various base fluid and nanoparticle shape factor. *Int J Numer Meth Heat Fluid Flow* 2021;31:402-417. [\[CrossRef\]](#)
- [34] Kolade Koriko O, Oreyeni T, John Omowaye A, Lare Animasaun I. Homotopy analysis of MHD free convective micropolar fluid flow along a vertical surface embedded in non-darcian thermally-stratified medium. *Open J Fluid Dyna* 2016;06:198-221. [\[CrossRef\]](#)
- [35] Cortell R. Heat and fluid flow due to non-linearly stretching surfaces. *Appl Math Comp* 2011;217:7564-7572. [\[CrossRef\]](#)
- [36] Waini I, Ishak A, Pop I. Hybrid nanofluid flow and heat transfer over a nonlinear permeable stretching/shrinking surface. *Int J Numer Meth Heat Fluid Flow* 2019;29:3110-3127. [\[CrossRef\]](#)
- [37] Abu-Nada E. Application of nanofluids for heat transfer enhancement of separated flows encountered in a backward facing step. *Int J Heat Fluid Flow* 2008;29:242-249. [\[CrossRef\]](#)
- [38] Sheikholeslami M, Hatami M, Ganji DD. Nanofluid flow and heat transfer in a rotating system in the presence of a magnetic field. *J Molecular Liquids* 2014;190:112-120. [\[CrossRef\]](#)
- [39] Gamachu D, Ibrahim W. Mixed convection flow of viscoelastic Ag-Al₂O₃/water hybrid nanofluid past a rotating disk. *Phys Scr* 2021;96:125205. [\[CrossRef\]](#)
- [40] Gangadhar K, Edukondala Nayak R, Venkata Subba Rao M, Kannan T. Nodal/saddle stagnation point slip flow of an aqueous convective magnesium oxide-gold hybrid nanofluid with viscous dissipation. *Arab J Sci Engineer* 2021;46:2701-2710. [\[CrossRef\]](#)
- [41] Khashiie NS, Arifin NM, Wahid NS, Pop I. Insight into unsteady separated stagnation point flow of hybrid nanofluids subjected to an electro-magneto-hydrodynamics riga plate. *Magnetochemistry* 2023;9:9020046. [\[CrossRef\]](#)
- [42] Waqas H, Raza Shah Naqvi SM, Alqarni MS, Muhammad T. Thermal transport in magnetized flow of hybrid nanofluids over a vertical stretching cylinder. *Case Stud Therm Engineer* 2021;27:101219. [\[CrossRef\]](#)
- [43] Eldabe NT, Gabr ME, Ali KK, Abdelzaher S, Zaher AZ. Mathematical modeling of the gyrotactic microorganisms of non darcian micropolar fluid containing different nanoparticles. *Chiang Mai J Sci* 2021;48:1412-1429.
- [44] Algehyne EA, Haq I, Raizah Z, Alduais FS, Saeed A, Galal AM. A passive control strategy of a micropolar hybrid nanofluid flow over a convectively heated flat surface. *J Magnet Magnet Mater* 2023;567:170355. [\[CrossRef\]](#)
- [45] Aman F, Ishak A, Pop I. Mixed convection boundary layer flow near stagnation-point on vertical surface with slip. *Appl Math Mech* 2011;32:1599-1606. [\[CrossRef\]](#)
- [46] Lok YY, Amin N, Pop I. Unsteady mixed convection flow of a micropolar fluid near the stagnation point on a vertical surface. *Int J Therm Sci* 2006;45:1149-1157. [\[CrossRef\]](#)
- [47] Uddin N, Alim A, Rahman M. MHD effects on mixed convective nanofluid flow with viscous dissipation in surrounding porous medium. *J Appl Math Phys* 2019;7:968-982. [\[CrossRef\]](#)
- [48] Devi GL, Niranjana H. Effects of MHD and electro-magnetic fields in nanofluid over a stretching sheet. *Solid State Technol* 2020;63:23026-23041.